

STEREO CORRESPONDENCE MATCHING: BALANCED MULTIWAVELETS VERSUS UNBALANCED MULTIWAVELETS

¹ Pooneh Bagheri Zadeh and ² Cristian V. Serdean

Department of Engineering, De Montfort University
The Gateway, Leicester, LE1 9BH, United Kingdom
phone: +44 (0)116 257 7691, fax: +44 (0)116 257 7692, emails: ¹pbz@dmu.ac.uk, ²cvs@dmu.ac.uk,
web: <http://www.dmu.ac.uk/>

ABSTRACT

This paper investigates the efficiency of unbalanced versus balanced multiwavelets in stereo correspondence matching. A multiwavelet transform is first applied to a pair of stereo images to decorrelate them into a number of subbands. Information in the approximation subbands of an unbalanced multiwavelet carries different spectral content of the input image while the balanced multiwavelet approximation subbands produce similar spectral content of the input image. Hence, the application of the approximation subbands of the unbalanced multiwavelets in disparity map generation could produce more accurate results compared to that of balanced multiwavelets. A global error energy minimization technique is employed to generate a disparity map for each approximation subband. The information in the resulting disparity maps is then combined using a Fuzzy algorithm to generate a dense disparity map. Simulation results show that the unbalanced multiwavelets produce a smoother disparity map with less mismatch errors compared to that of balanced multiwavelets.

1. INTRODUCTION

Stereo correspondence matching is a long-standing topic, which has attracted much research interest over the past decades. In stereo correspondence matching algorithms, the best correspondence points between the images taken at the same time but from slightly different viewpoints are found and used to generate a disparity map. The disparity map along with the stereo camera parameters are then used to calculate a depth map and produce a 3D view of the scene. However, finding the correct corresponding points between the two views poses a number of potential problems such as occlusion, ambiguity, illumination variation and radial distortion [1].

The correspondence matching algorithms are categorized into area-based (local) and energy-based (global) algorithms. In area-based methods a disparity vector for each pixel within a window search area is calculated using a matching algorithm while in energy-based methods, the disparity vector is determined using a global cost function minimization technique. The area-based methods are fast but they produce descent results, while global methods are time consuming and generating more accurate results.

Stefano et al [2] proposed an area-based correspondence matching method which is based on the uniqueness and constraint and relies on the left-to-right matching phase. Yoon et al [3] introduced a correlation (local) based correspondence matching technique, which uses a refined implementation of the Sum of Absolute Differences (SAD) criteria and a left-right consistency check. This algorithm uses a variable correlation window size to reduce the errors in the areas containing blurring or mismatch errors. Another local-based algorithm was reported by Yoon and Kweon [4], which uses different supporting weights based on the color similarity and geometric distances for each pixel in the search area to reduce the ambiguity errors.

Ogale and Aloimonos [5] proposed a global-based correspondence matching algorithm, which is independent of the contrast variation of the stereo images. This algorithm relies on multiple spatial frequency channels for local matching and a fast non-iterative left/right diffusion process for the global solution. An energy-based algorithm for stereo matching, which uses a belief propagation algorithm, was presented in [6]. This algorithm uses a hierarchical belief propagation to iteratively optimize the smoothness of the disparity map. It delivers a fast convergence by removing redundant computations. Choi and Jeong [7] proposed an energy-based stereo matching technique, which models the intensity differences between the two stereo images using a uniform local bias assumption. This local bias assumption is less sensitive to intensity dissimilarity between the stereo images when the normalized cross correlation matching cost function is used. The resulting information from the cost function and the fast belief propagation algorithm are combined to generate a smooth disparity map.

Recently, multiresolution based stereo correspondence matching algorithms have received much attention due to the hierarchical and scale-space localization properties of the wavelets [8-10]. This allows for correspondence matching to be performed on a coarse-to-fine basis, resulting in decreased computational costs. Sarkar and Bansal [9] presented a multiresolution based correspondence matching technique using a mutual information algorithm. They showed that the multiresolution technique produces significantly more accurate matching results compared to correlation based algorithms with less computational cost.

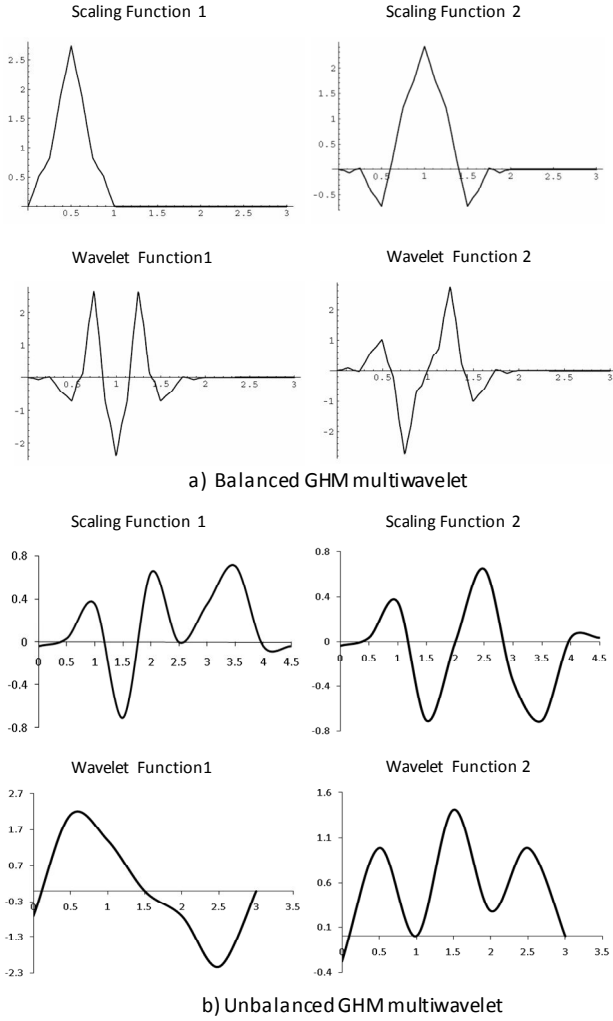


Figure 1 – GHM multiwavelet with multiplicity 2 and approximation order 2: a) balanced, b) unbalanced.

Research has shown that unlike scalar wavelets, multiwavelets can possess orthogonality (preserving length), symmetry (good performance at the boundaries via linear-phase), and a high approximation order at the same time [11], which could potentially increase the accuracy of the correspondence matching techniques. In spite of their highly desirable advantages compared to scalar wavelets, multiwavelets have been little investigated in the literature for stereo correspondence matching. Bhatti and Nahavandi [10] proposed a multiwavelet based stereo correspondence matching algorithm. In the matching process, they use wavelet transform modulus maxima as the matching feature in the coarse level to generate a disparity map. This is then followed by the coarse to fine strategy to refine the disparity map up to the finest level.

This paper investigates the use of balanced and unbalanced multiwavelet transforms in stereo correspondence matching. A multiwavelet transform (either balanced or unbalanced) is applied to the input stereo images to decompose them into their subbands. A global error energy minimization algorithm is then employed to generate a disparity map for each of the approximation subbands. A fuzzy algorithm is

then used to combine the resulting disparity maps and generate a dense disparity map.

The rest of the paper is organized as it follows. Section 2 presents a brief review of the multiwavelet transform. The proposed stereo matching technique is discussed in Section 3. Experimental results are presented in Section 4 and the paper is concluded in Section 5.

2. MULTIWAVELET TRANSFORM

Multiwavelet transforms operate on a similar principle to scalar wavelets and can be considered as a multichannel version of scalar wavelets. Classical wavelet theory is based on the refinement equations as given below:

$$\begin{aligned}\phi(t) &= \sum_{k=-\infty}^{k=\infty} h_k \phi(m t - k) \\ \psi(t) &= \sum_{k=-\infty}^{k=\infty} g_k \psi(m t - k)\end{aligned}\quad (1)$$

where $\phi(t)$ is a scaling function, $\psi(t)$ is a wavelet function, h_k and g_k are scalar filters and m represents the subband number. In contrast to the wavelet transform, multiwavelets have two or more scaling and wavelet functions. The set of scaling and wavelet functions of a multiwavelet in vector notation can be defined as:

$$\begin{aligned}\Phi(t) &\equiv [\phi_1(t) \ \phi_2(t) \ \phi_3(t) \ \dots \ \phi_r(t)]^T \\ \Psi(t) &\equiv [\psi_1(t) \ \psi_2(t) \ \psi_3(t) \ \dots \ \psi_r(t)]^T\end{aligned}\quad (2)$$

where $\Phi(t)$ and $\Psi(t)$ are the multi-scaling function and respectively the multiwavelet function, with r scaling and wavelet functions. A multiwavelet with two scaling and wavelet functions can be defined in a similar fashion to the wavelet transform given in equation (1) as shown in [12]:

$$\begin{aligned}\Phi(t) &= \sqrt{2} \sum_{k=-\infty}^{k=\infty} H_k \Phi(m t - k) \\ \Psi(t) &= \sqrt{2} \sum_{k=-\infty}^{k=\infty} G_k \Psi(m t - k)\end{aligned}\quad (3)$$

where H_k and G_k are $r \times r$ matrix filters and m is the subband number. In the case of scalar wavelets $r=1$, while multiwavelets support $r \geq 2$. In this paper the value of r restricts to 2. Figure 1 shows an example of GHM balanced and unbalanced multiwavelet basis functions with multiplicity $r=2$ and approximation order 2 [11, 13].

Similar to wavelet transforms, multiwavelets can be implemented using Mallat's filter bank theory [8]. Figure 2 shows the analysis and synthesis stages for a 1-D multiwavelet transform and one level decomposition, where blocks G and H are the low-pass and high-pass analysis filters and \tilde{G} and \tilde{H} are the low-pass and high-pass synthesis filters. The multiwavelet transform is separable, hence a 2D multiwavelet transform can be calculated via two successive 1D multiwavelet transforms, first

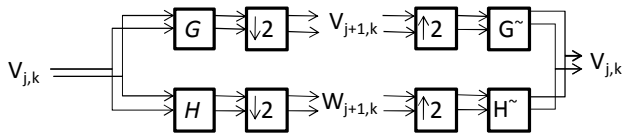


Figure 2 – Analysis/synthesis stage of a one level multiwavelet transform.

performed on the image rows and then performed on the resulting columns. Therefore, by applying a one level 2D multiwavelet with multiplicity of 2, sixteen subbands are generated, which four are approximation subbands. Multiwavelets support symmetry, orthogonality and approximation order higher than 1 simultaneously, while scalar wavelet does not allow these extra degree of freedom. Synthesis and analysis stage of a multiwavelet with multiplicity 2 produces four different approximation subbands. Analysis filter banks that multiwavelet transforms usually use have poor frequency characteristics. Therefore the approximation subbands contains some of the high frequency information. In the case of unbalanced multiwavelets, the resulting approximation subbands carry different spectral content of the image information, while the balanced multiwavelets approximation subband produce similar spectral content of the original image [17]. This feature of unbalanced multiwavelets has the potential to increase the accuracy of the calculated disparity maps and reduce the number of erroneous matches compared to that of balanced multiwavelets. Figure 3 gives a visual comparison of the resulting subbands for the Antonini 9/7 scalar wavelet, as well as for the balanced and unbalanced GHM multiwavelets applied to Lena test image. The results are shown in Figures 3(a) to 3(c). As it can be seen from Figure 3, multiwavelets generate four subbands instead of each subband that a wavelet creates. The resulting unbalanced multiwavelet subbands carry different spectral content of the original Lena test image, while the balanced multiwavelet subbands produce similar spectral content of the Lena test image. More information about the generation of multiwavelets, their properties and their applications can be found in [11-13].

3. MULTIWAVELET BASED STEREO MATCHING TECHNIQUE

A block diagram of the multiwavelet based stereo matching technique using the global error energy minimization algorithm is illustrated in Figure 4. A pair of stereo images is input to the stereo matching system. The images are first rectified to suppress the vertical displacement. A multiwavelet transform is then applied to the input stereo images which decomposes them into their subbands as shown in Figure 5, where $L_x L_y$ represent the approximation subbands and $L_x H_y$, $H_x L_y$ and $H_x H_y$ are the detail subbands, with $x = \overline{1, 2}$ and $y = \overline{1, 2}$. For the propose of this paper, only one level of decomposition is used. The pre-filtering process used in this paper is a repeat row type, which means that after one level of decomposition, the resulting

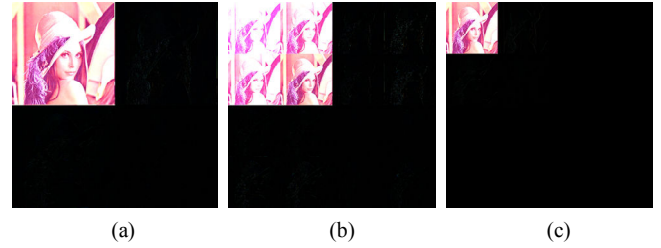


Figure 3 – Single level decomposition of Lena test image (a) Antonini 9/7 wavelet transform, (b) balanced GHM multiwavelet transform and (c) unbalanced GHM multiwavelet transform.

size of the four approximation subbands will be the same as the size of the original image. In the case of the unbalanced multiwavelet, each of the four resulting LL subbands is an approximation of the input image with different spectral content of the input image, while the resulting LL subbands of the balanced multiwavelet carry similar spectral content of the input image. In addition to this, the information in the approximation subbands is less sensitive to the shift variability of the multiwavelets. Hence, approximation subbands are used to generate the correspondence matching. The same approximation subbands in the two images are then passed to a regional based stereo matching block. The matching algorithm uses a global error energy minimization technique [14] to generate a disparity map between the two input subbands. This global error energy minimization technique is briefly described in subsection 3.1. The matching process outputs four disparity maps. These maps are then combined using a Fuzzy algorithm to generate a dense disparity map which reduces the number of erroneous matches.

3.1 Global Error Energy Minimization technique

The Global Error Energy Minimization (GEEM) technique [14] calculates a disparity vector for each pixel. It searches for the best match for each pixel in the correspondence search area of the other image using an error minimization criterion. For RGB images, the error energy criterion can be defined as:

$$Er_{en}(i, j, w_x, w_y) = \frac{1}{3} \sum_{k=1}^3 (I_1(i+w_x, j+w_y, k) - I_2(i, j, k))^2$$

$$\begin{cases} -d_x \leq w_x \leq d_x & \text{and} & -d_y \leq w_y \leq d_y \\ i = 1, \dots, m & \text{and} & j = 1, \dots, n \end{cases} \quad (4)$$

where I_1 and I_2 are the two input images, $Er_{en}(i, j, w_x, w_y)$ is the energy difference of the pixel $I_2(i, j)$ and pixel $I_1(i+w_x, j+w_y)$, d_x and d_y are the maximum displacements around the pixel in the x and respectively y directions, m and n are the image size and k represents the three components of an RGB image.

In order to determine the disparity vector for each pixel in the current view, the GEEM algorithm first calculates Er_{en} of each pixel with all the pixels in its search area in the

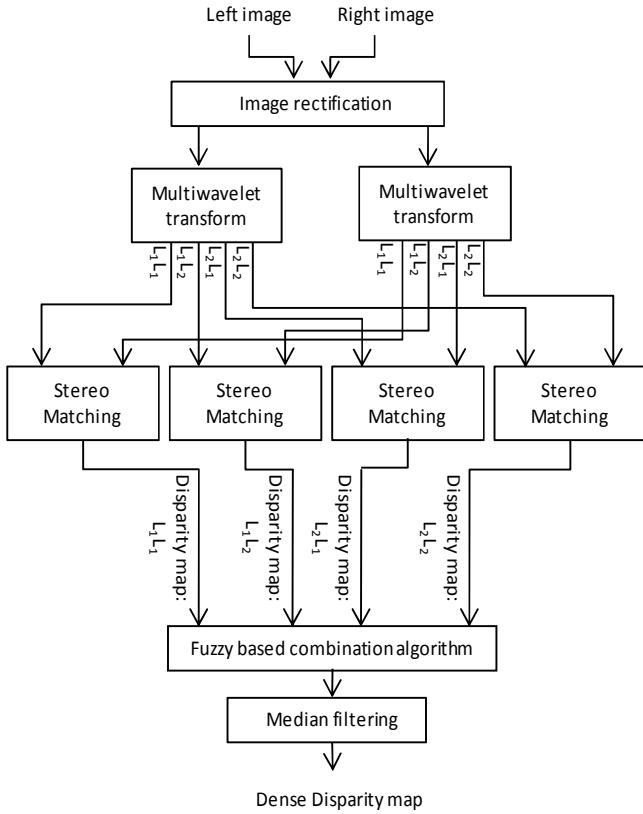


Figure 4 – Block diagram of the multiwavelet based stereo matching technique using the global error energy minimization algorithm.

correspondence image. For every disparity vector (w_x, w_y) in the disparity search area, the energy of the error is calculated using equation (4) and placed into a matrix. Each of the resulting energy error matrices is first filtered using an average filter to decrease the number of incorrect matches [15]. The disparity index of each pixel is then determined by finding the disparity index of the matrix which contains the minimum energy error for that pixel. In order to increase the reliability of the disparity vectors around the object boundaries, which is the result of object occlusion in images, the generated disparity map undergoes a thresholding procedure as it follows:

$$\tilde{d}(i, j) = \begin{cases} d(i, j) & Er_{en}(i, j) \leq \alpha \times Mean(Er_{en}) \\ 0 & Er_{en}(i, j) > \alpha \times Mean(Er_{en}) \end{cases} \quad (5)$$

where $\tilde{d}(i, j)$ is the processed disparity map, $d(i, j)$ is the

L_1L_1	L_1L_2	L_1H_1	L_1H_2
L_2L_1	L_2L_2	L_2H_1	L_2H_2
H_1L_1	H_1L_2	H_1H_1	H_1H_2
H_2L_1	H_2L_2	H_2H_1	H_2H_2

Figure 5 – Multiwavelet subband structure for one level of decomposition.

disparity map, α is a tolerance reliability factor, $Er_{en}(i, j)$ is the minimum error energy of the pixel (i, j) calculated and selected in the previous stage. Finally a median filter is applied to the processed disparity map, $\tilde{d}(i, j)$ to further smooth the disparity map.

4. SIMULATION RESULTS

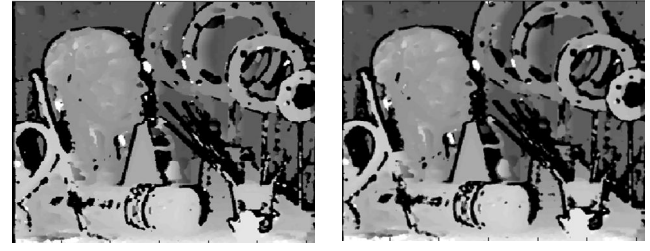
In order to investigate the performance of the unbalanced multiwavelet compared to the balanced multiwavelet, both balanced and unbalanced multiwavelets are employed in the proposed multiwavelet based GEEM technique. The resulting disparity maps from both balanced and unbalanced multiwavelets are compared to each other as well as to a similar algorithm operating in the spatial domain and in the wavelet domain. The results were generated using the 'Art' stereo test images from the Middlebury stereo database [16]. Figure 6 shows the left image and the ground truth of the test images. The experimental results were generated using the unbalanced GHM multiwavelet, balanced GHM multiwavelet and the Antonini 9/7 wavelet. Figures 7(a) to 7(d) show the resulting disparity maps using the multiwavelet subbands L_1L_1, L_1L_2, L_2L_1 and L_2L_2 , respectively. In order to give a visual comparison, the resulting disparity maps using the proposed multiwavelet based algorithm for both balanced and unbalanced GHM multiwavelets, the wavelet based GEEM algorithm and the GEEM technique applied to the original stereo views, are illustrated in Figures 8(a) to 8(d), respectively. In these figures areas with intensity zero represent unreliable disparities. From Figure 8, it is clear that the unbalanced multiwavelet based algorithm produces a more accurate and smoother disparity map compared to the similar balanced multiwavelet- and wavelet-based technique and also the GEEM algorithm in the spatial domain. This can be explained by the different spectral content of the approximation subbands of the unbalanced multiwavelet. This feature of unbalanced multiwavelets enables the global error energy minimization algorithm to generate more reliable matches from the four unbalanced multiwavelet approximation subbands, compared to using balanced multiwavelets, scalar wavelets and/or the spatial domain.

5. CONCLUSION

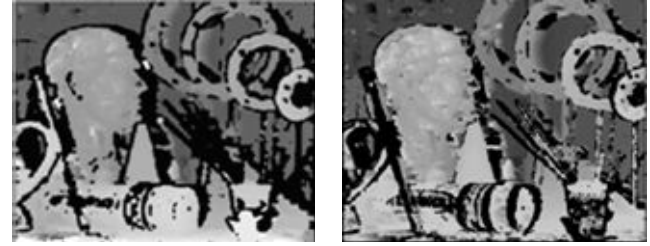
In this paper, we presented an investigation on the efficiency of the unbalanced multiwavelets compared to balanced multiwavelets in stereo correspondence. A stereo correspondence matching technique using a global error energy minimization algorithm was employed for the propose of this investigation. For one level of decomposition, a multiwavelet transform (either balanced or unbalanced) with multiplicity of 2 was applied to a pair of stereo test images. The resulting four approximation subbands of the two views were employed to generate the disparity maps using the global error energy minimization algorithm. The resulting four disparity maps were then combined using a Fuzzy algorithm. Results show that the proposed unbalanced multiwavelet based technique produces a disparity map with



Figure 6 – The left image and the ground truth of the 'Art' stereo images.

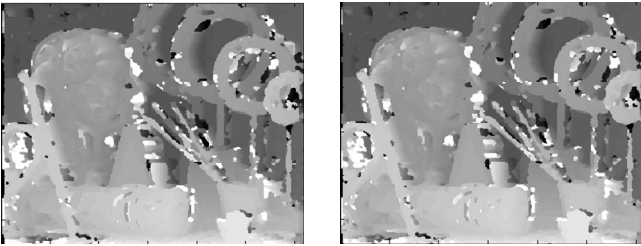


(a) (b)

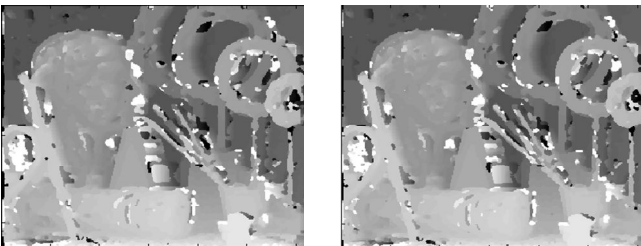


(c) (d)

Figure 8 – Disparity maps using global error energy minimization algorithm: a) with unbalanced multiwavelet, b) with balanced multiwavelet, c) in the wavelet domain and d) in the spatial domain.



(a) (b)



(c) (d)

Figure 7 – Disparity maps using the multiwavelet approximation subbands: a) L_1L_1 , b) L_1L_2 , c) L_2L_1 and d) L_2L_2 .

significantly less mismatch errors compared to the global error energy minimization algorithm applied to the original image data in the spatial domain or the balanced multiwavelet transformed and wavelet transformed image data.

REFERENCES

- [1] D. Scharstein and R. Szeliski, "A Taxonomy and Evaluation of Dense Two-Frame Stereo Correspondence Algorithms," *Int. Jour. Comp. Vision*, vol. 47, pp. 7-42, Apr.2002.
- [2] L. Di Stefano, M. Marchionni, S. Mattoccia, G. Neri, "A Fast Area-Based Stereo Matching Algorithm," *Image and vision computing*, vol. 22, pp. 983-1005, March 2004.
- [3] S. Yoon, S. K. Park, S. Kang and Y. Kwak, "Fast correlation-based stereo matching with the reduction of systematic errors," *Patt. Recog. Let.*, vol.26, pp. 2221-2231, Oct.2005.
- [4] K.J. Yoon and I. S. Kweon, "Adaptive support-weight approach for correspondence search," *IEEE Tran. Pattern Analysis Machine Intel.*, vol. 28, pp. 650-656, April 2006.
- [5] A.S. Ogale and Y. Aloimonos, "Robust Contrast Invariant Stereo Correspondence," *Proc. IEEE Int. Conf. on Robotics and Automation*, pp. 819-824, April 2005.
- [6] Q. Yang, L. Wang, R. Yang, S Wang, M. Liao, D. Nister, "Real-time global stereo matching using hierarchical belief propagation", In Proc. of BMVC 2006.
- [7] I. Choi and H. Jeong, "Fast Belief Propagation for Real-time Stereo Matching," *Int. Conf. on Advanced Communication Tech., ICACT 2009*, pp. 1175-1179, February 2009.
- [8] S. Mallat, *A Wavelet Tour of Signal Processing*, Academic Press, 1999.
- [9] I. Sarkar, M. Bansal, "A wavelet-based multiresolution approach to solve the stereo correspondence problem using mutual information," *IEEE Trans. on system, man, and cybernetics*, vol. 37, pp. 1009-1014, August 2007.
- [10] A. Bhatti and S. Nahvandi, "Depth estimation using multi-wavelet analysis based stereo vision approach," *Proc. of Int. Conf. on Wavelet Analysis and Pattern Recognition*, pp. 1471-1476, Nov. 2007.
- [11] V. Strela and A.T. Walden, "Signal and image denoising via wavelet thresholding: orthogonal and biorthogonal, scalar and multiple wavelet transforms," *In Nonlinear and Nonstationary Signal Processing*, pp. 124-157, 1998.
- [12] V. Strela, "Multiwavelets: theory and applications," PhD thesis, MIT, 1996.
- [13] J. Lian and C. K. Chui, "Balanced Multiwavelets With Short Filters," *IEEE Signal Processing Letters*, vol. 11, no. 2, pp. 75-78, Feb. 2004
- [14] B. B. Alagoz, "Obtaining depth maps from colour images by region based stereo matching algorithms," *On-cuBilim Algorithm and Sys. Labs*, vol. 08, Art.No:04, 2008.
- [15] R.C. Gonzalez, R.E. Woods, S.L. Eddins, *Digital image processing second edition*, Prentice Hall, pp. 75-142, 2002.
- [16] <http://vision.middlebury.edu/stereo/>
- [17] L. Ghouti, A. Bouridane, M. K. Ibrahim, and S. Bousakta, "Digital Image Watermarking Using Balanced Multiwavelets," *IEEE Trans. on Signal Proc.*, Vol. 54, no. 4, pp. 1519-1536, April 2006.